The Observation of Up-going Charged Particles Produced by High Energy Muons in Underground Detectors

The MACRO Collaboration

M. Ambrosio[12], R. Antolini[7], C. Aramo[7,p], G. Auriemma[14,a], A. Baldini[13], G. C. Barbarino[12], B. C. Barish[4], G. Battistoni[6,b], R. Bellotti[1], C. Bemporad[13], P. Bernardini[10], H. Bilokon[6], V. Bisi[16], C. Bloise[6], C. Bower[8], S. Bussino[14], F. Cafagna[1], M. Calicchio[1], D. Campana[12], M. Carboni[6], M. Castellano[1], S. Cecchini[2,c], F. Cei[13,d], V. Chiarella[6], S. Coutu[11], G. Cunti[14], L. De Benedictis[1], G. De Cataldo[1], H. Dekhissi[2,e], C. De Marzo[1], I. De Mitri[9], M. De Vincenzi[14,f], A. Di Credico[7], O. Erriquez[1], C. Favuzzi[1], C. Forti[6], P. Fusco[1], G. Giacomelli[2], G. Giannini[13,g], N. Giglietto[1], M. Grassi[13], L. Gray[4,7], A. Grillo[7], F. Guarino[12], P. Guarnaccia[1], C. Gustavino[7], A. Habig[3], K. Hanson[11], A. Hawthorne[8], R. Heinz[8], E. Iarocci[6,h], E. Katsavounidis[4], E. Kearns[3], S. Kyriazopoulou[4], E. Lamanna[14], C. Lane[5], D. S. Levin[11], P. Lipari[14], N. P. Longley[4,m], M. J. Longo[11], F. Maaroufi[2,e], G. Mancarella[10], G. Mandrioli[2], S. Manzoor[2,n], A. Margiotta Neri[2], A. Marini[6], D. Martello[10,], A. Marzari-Chiesa[16], M. N. Mazziotta[1], C. Mazzotta[10], D. G. Michael[4], S. Mikheyev[7,i], L. Miller[8], P. Monacelli[9], T. Montaruli[1], M. Monteno[16], S. Mufson[8], J. Musser[8], D. Nicoló[13,d], R. Nolty[4], C. Okada[3], C. Orth[3], G. Osteria[12], O. Palamara[10], V. Patera[6,h], L. Patrizii[2], R. Pazzi[13], C. W. Peck[4], S. Petrera[9], P. Pistilli[14,f], V. Popa[2,l], V. Pugliese[14], A. Rainó[1], J. Reynoldson[7], F. Ronga[6], U. Rubizzo[12], A. Sanzgiri[15], C. Satriano[14,a], L. Satta[6,h], E. Scapparone[7], K. Scholberg[3,4], A. Sciubba[6,h], P. Serra-Lugaresi[2], M. Severi[14], M. Sioli[2], M. Sitta[16], P. Spinelli[1], M. Spinetti[6], M. Spurio[2], R. Steinberg[5], J. L. Stone[3], L. R. Sulak[3], A. Surdo[10], G. Tarlé[11], V. Togo[2], C. W. Walter[3,4] and R. Webb[15]

1. Dipartimento di Fisica dell'Università di Bari and INFN, 70126 Bari, Italy
2. Dipartimento di Fisica dell'Università di Bologna and INFN, 40126 Bologna, Italy
3. Physics Department, Boston University, Boston, MA 02215, USA
4. California Institute of Technology, Pasadena, CA 91125, USA
5. Department of Physics, Drexel University, Philadelphia, PA 19104, USA
6. Laboratori Nazionali di Frascati dell'INFN, 00044 Frascati (Roma), Italy
7. Laboratori Nazionali del Gran Sasso dell'INFN, 67010 Assergi (L'Aquila), Italy
8. Depts. of Physics and of Astronomy, Indiana University, Bloomington, IN 47405, USA
9. Dipartimento di Fisica dell'Università dell'Aquila and INFN, 67100 L'Aquila, Italy
10. Dipartimento di Fisica dell'Università di Lecce and INFN, 73100 Lecce, Italy
11. Department of Physics, University of Michigan, Ann Arbor, MI 48109, USA
12. Dipartimento di Fisica dell'Università di Napoli and INFN, 80125 Napoli, Italy
13. Dipartimento di Fisica dell'Università di Pisa and INFN, 56010 Pisa, Italy
14. Dipartimento di Fisica dell'Università di Roma "La Sapienza" and INFN, 00185 Roma, Italy
15. Physics Department, Texas A&M University, College Station, TX 77843, USA
16. Dipartimento di Fisica Sperimentale dell'Università di Torino and INFN, 10125 Torino, Italy

a Also Università della Basilicata, 85100 Potenza, Italy

b Also INFN Milano, 20133 Milano, Italy
c Also Istituto TESRE/CNR, 40129 Bologna, Italy
d Also Scuola Normale Superiore di Pisa, 56010 Pisa, Italy
e Also Faculty of Sciences, University Mohamed I, B.P. 424 Oujda, Morocco
f Also Dipartimento di Fisica, Università di Roma Tre, Roma, Italy
g Also Università di Trieste and INFN, 34100 Trieste, Italy
h Also Dipartimento di Energetica, Università di Roma, 00185 Roma, Italy
i Also Institute for Nuclear Research, Russian Academy of Science, 117312 Moscow, Russia
l Also Institute for Space Sciences, 76900 Bucharest, Romania
m Swarthmore College, Swarthmore, PA 19081, USA
n RPD, PINSTECH, P.O. Nilore, Islamabad, Pakistan
p Also INFN Catania, 95129 Catania, Italy

Abstract

An experimental study of the production of up-going charged particles in inelastic interactions of down-going underground muons is reported, using data obtained from the MACRO detector at the Gran Sasso Laboratory. In a sample of 12.2×10^6 single muons, corresponding to a detector livetime of 1.55 y, 243 events are observed having an up-going particle associated with a down-going muon. These events are analysed to determine the range and emission angle distributions of the up-going particle, corrected for detection and reconstruction efficiency.

Measurements of the muon neutrino flux by underground detectors are often based on the observation of through-going and stopping muons produced in ν_μ interactions in the rock below the detector. Up-going particles produced by an undetected down-going muon are a potential background source in these measurements. The implications of this background for neutrino studies using MACRO are discussed.

1. Introduction

One of the primary goals of the MACRO detector at the Gran Sasso underground laboratory is the measurement of the flux of atmospheric muon neutrinos. In this paper we present the measurement of a potential background in these studies; charged up-going particles (primarily pions) produced in inelastic interactions of down-going muons in the rock surrounding the detector. If the down-going muon is not detected the up-going pion may be misidentified as resulting from a neutrino-induced event. This will occur, for example, when the μ passes near but not through the detector. This type of event, therefore, represents a background in the measurement of the flux of neutrino-induced upward through-going and stopping muons. The events under study, although similar in topology to muon backscattering, have an observed rate which is many orders of magnitude larger than that expected from the large angle scattering of muons [1, 2]. The relatively low energy up-going tracks are primarily charged pions produced in hard muon scattering on a nucleon N, $\mu + N \rightarrow \mu + \pi^{\pm} + X$. Hadron production by underground muons has been recently discussed [3] in conjunction with the problem of neutron background in the measurement of the ν_e/ν_μ atmospheric neutrinos ratio by large water Cherenkov detectors [4]. Hadron production by muon interactions in matter is also a source of background in radiochemical solar neutrino experiments [5].

In this paper we present the results of a study of these events carried out with the MACRO detector. In Section 2 the MACRO apparatus and the method used to identify muon-induced up-going charged particles are described. The details of the analysis of the data are given in Section 3. In Section 4 the observed range and emission angle distributions for the up-going particle are presented. In Section 5 the detector response and the tracking efficiency for these events are calculated. In Section 6 the results are interpreted within the framework of a model of the photonuclear interactions of high energy muons provided by the FLUKA generator. Finally, in Section 7 the background due to up-going particles produced by hard muon scattering in the measurement of neutrino-induced muons is calculated for the MACRO experiment.

2. Muon-induced Up-going Particles in MACRO.

The MACRO detector, described in detail in Ref. [6], is located in Hall B of the Gran Sasso underground laboratory. The detector has global dimensions of $76.6m \times 12m \times 9.3m$, and is divided longitudinally in six similar supermodules and vertically in a lower ($4.8\ m$ high) and an upper part ($4.5\ m$ high). The active detectors include horizontal and vertical planes of limited streamer tubes for particle tracking, and liquid scintillation counters for fast timing. In the lower part, the eight inner planes of limited streamer tubes are separated by passive absorber (iron and rock $\sim 60 g\ cm^{-2}$) in order to set a minimum threshold of $\sim 1\ GeV$ for vertical muons crossing the detector. The upper part of the detector is an open volume containing electronics and other equipment. The horizontal streamer tube planes are instrumented with external pick-up strips at an angle of 26.5^o with respect to the streamer tube's wire, providing stereo readout of the detector hits. The transit time of particles through the detector is obtained from the scintillation counters by measuring the mean time at which signals are observed at the two ends of each counter, and taking the difference in the measured mean time between

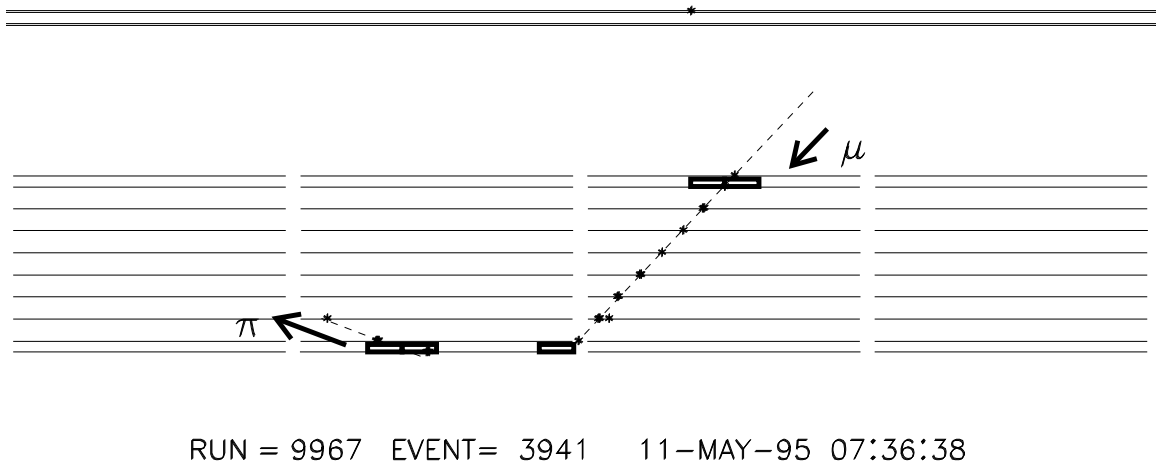

Figure 1: On-line display of a typical muon interaction in the rock below the apparatus giving rise to an up-going charged particle. The rectangular boxes indicate scintillator counter hits and the points are streamer tube hits. The tracks are shown in the wire view of the streamer tubes. Only two supermodules are drawn.

upper and lower counters. The particle direction in the detector is given by the sign of this difference.

The apparatus can observe charged particles produced at large angles by hard muon interactions if the reaction happens either inside the apparatus or in the rock and concrete below the apparatus. In the latter case, a secondary particle produced at a large angle in the reaction is seen as an up-going particle in the apparatus (see Fig. 1). If the muon passes through the detector, such an event consists of two tracks converging somewhere below the detector, both in the wire and strip projective views of the tracking system. The secondary particle reaches the scintillator counters with a positive time delay with respect to the counters hit by the muon.

In the sample of muon plus up-going pion events, the down-going particle is usually the longer of the two tracks, and is reconstructed by the standard MACRO tracking procedure [6]. This tracking algorithm is optimized for the reconstruction of single and multiple muon events, and requires that at least four central streamer tube planes are crossed by the particle, corresponding to a minimum of ~ 200 $g\ cm^{-2}$ of detector grammage traversed. For this study, a tracking algorithm was developed to reconstruct the short, diverging tracks characteristic of the events of interest. This algorithm searches for alignments between a cluster of scintillation counters and at least two streamer tube hits in a 4 meter wide region centered on the counter cluster. The scintillator cluster is defined as a contiguous group of neighboring counters simultaneously hit by one or more particles. The reconstructed coordinates of the scintillation cluster, obtained from the identity of the hit counters and the timing difference between the two ends of the counters, are used by the tracking algorithm as an additional track point. A track candidate consists of an alignment between at least three hits in a 4 meter wide region, and is referred to below as a short track. The minimum vertical depth for events reconstructed by this algorithm is approximately 25 $g\ cm^{-2}$.

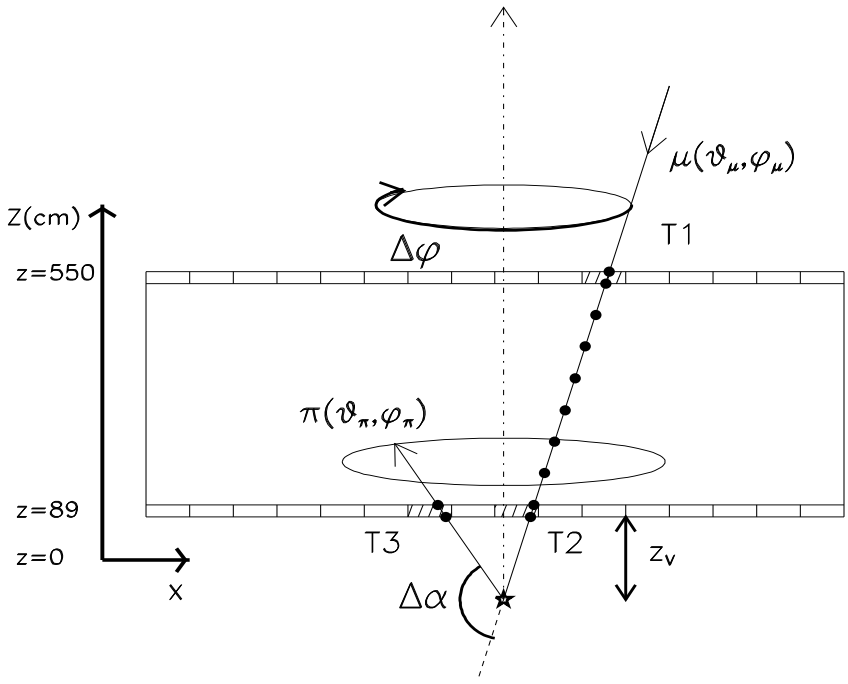

Figure 2: Sketch of an event containing a down-going muon with direction $(\vartheta_\mu, \varphi_\mu)$ producing an up-going pion with direction $(\vartheta_\pi, \varphi_\pi)$. The arrows indicate the direction of the particles, deduced from the timing information obtained from the scintillation counters (T_1, T_2 and T_3). The filled points correspond to the streamer tube hits. The zenith and azimuth emission angles $\Delta\alpha, \Delta\varphi$ of the pion with respect to the muon direction are indicated.

3. Event Selection

The data sample used in this study includes events in which a single muon is reconstructed by the standard tracking algorithm (see Fig. 2, for a sketch). The short track algorithm is then used to search for events in which a secondary up-going pion enters the detector from below and crosses the bottom layer of scintillator counters and at least two streamer tube planes before coming to rest in the detector. Finally, the timing information from the scintillation counters is used to identify the direction of the two particles. As demonstrated below, the pion and the muon are resolved with high efficiency if the wire hits belonging to the two tracks are separated by at least $\sim 75\ cm$.

Two different data periods have been analyzed. In the first (sample A, from December 1992 through June 1993), the upper part of the apparatus was not in acquisition. In the second period (sample B, from April 1994 until January 1996) the entire apparatus, including the upper part was in acquisition. Table 1 contains the detector livetime, the number of single downgoing muons, the number of reconstructed short tracks, and the number of final muon plus up-going pion events obtained in the two data taking periods. As shown in the table, a short track is reconstructed in 31717 of the 12.2×10^6 single muon events. These are referred to below as double track events. A visual scan of a subsample of 15% of these events has been performed to determine their nature. In the most common case (76% of events in sample A, and 69% in sample B), the short track in the event belongs to a second downgoing muon, parallel to the first. The difference in the fraction of events of this type between the two data samples is due to the improved acceptance for double muon events during the period in which the entire apparatus was in acquisition. Other topologies, all producing an incorrectly reconstructed short track, are due to electromagnetic showers inside the detector (17% of events in the two

Sample	Single downgoing muons	Double tracks	Livetime (h)	Down muon + up pion
A	$3.3 \cdot 10^6$	12216	4235	65
B	$8.9 \cdot 10^6$	19501	9351	178
A+ B	$12.2 \cdot 10^6$	31717	13586	243

Table 1: Number of single down-going muons and of events with an additional short track (double tracks) in the two data periods A and B. In the fourth column the livetime (h) of the apparatus is shown. The number of identified muon plus up-going pion events is given in the last column.

periods), incorrect track point assignment (4%), muon interactions occurring inside the detector (5%) and low momentum muons undergoing significant multiple scattering in the detector (2%). In all of these event types the two reconstructed tracks do not possess a common vertex point below the detector.

The event topologies identified as background in the visual scan are rejected by applying the following analysis cuts to the sample of double track events. Double muon events are rejected by requiring that the direction of the two tracks differ by more than 26^o. Electromagnetic showers are rejected by requiring that the total number of streamer tube hits not belonging to the muon track be less than 20, while muon interactions inside the apparatus and low energy muons are rejected by requiring that the intersection point of the two tracks be outside the detector volume. 3467/31717 events pass these cuts and have been visually scanned to obtain the final data sample. Events eliminated in this final visual scan include in most cases multiple and/or wrongly reconstructed short tracks, produced by a double muon event or by a muon electromagnetic shower. As a result, 65 events in sample A and 178 in sample B are classified as muon plus up-going pion events.

The probability of rejecting a genuine muon plus up-going pion event through the software cuts has been evaluated by scanning a random subsample of 6200 double track events, representing ∼20% of the full double track event set, for muon plus up-going pion events. 54 events are found, of which 3 are rejected when the software cuts are applied. The corresponding selection efficiency is $\epsilon_s = 94\%$. An independent check of ϵ_s is obtained by applying the software cuts to the sample of simulated (discussed below) down-going muons plus up-going pions; 151/3347=4.5% of the simulated events are discarded. Based on the number of events in the final data sample, and a selection efficiency $\epsilon_s = 94\%$, the rate of detected up-going pions per down-going muon at the MACRO depth is:

$$n_{\pi/\mu} = \frac{243}{0.94 \times 12.2\ 10^6} = (2.1 \pm 0.2)\ 10^{-5} \qquad (1)$$

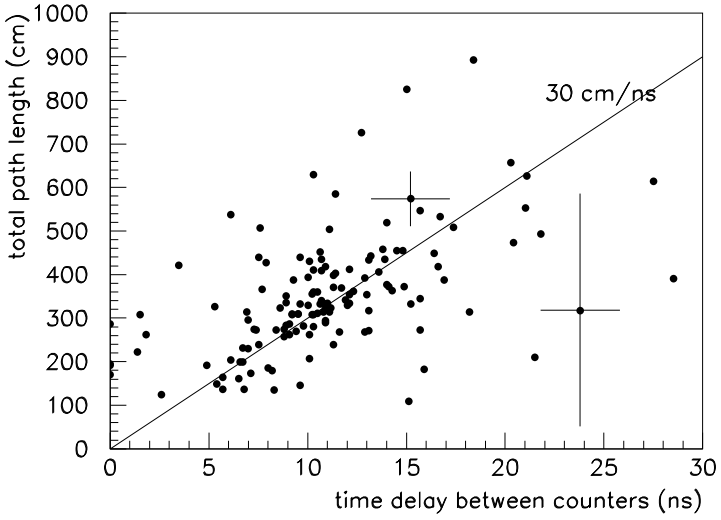

Figure 3: Total path length (see text) versus time delay $\Delta t = (T_3 - T_2)$ between scintillation counter hits in the bottom plane. Only the 168 events for which $|z_v^w - z_v^s| < 50\ cm$ are included. The large spread around the central line is due to the combined uncertainty in the total path length and timing reconstruction. As an example, error bars are drawn for two events. For three events, T_2 is missing and $\Delta t = 0$

4. Analysis

The 243 events in the final data sample are now used to obtain the distribution of the range of the up-going pion, the angle between the μ and π, and the radial distance D between the pion and the muon at a vertical position corresponding to the center of the bottom layer of scintillation counters.

Referring to Fig. 2, the point at which the muon interaction occurs, $\vec{x}_v = (x_v, y_v, z_v)$, is defined as the intersection of the observed muon and pion tracks. The vertex depth z_v is obtained separately in the wire (z_v^w) and strip (z_v^s) projection. In 75 of the 243 events in the final data set the difference between the vertex depth in the wire and strip views exceeds 50 cm; this event subsample is defined as poorly reconstructed in the following.

The timing information obtained from the scintillation counter system is used to determine the direction of motion of each particle, and as an independent check of the vertex location obtained from the tracking system. Using the convention of Fig. 2, a down-going particle will have a transit time difference $(T_2 - T_1) > 0$. The bottom counter crossed by the short track is reached at a time T_3, with $(T_3 - T_2) > 0$. For 206 of the 243 events in the final data sample the requirement $(T_3 - T_2) > 0$ is fulfilled. For the remaining 37 events, either the down-going muon misses the counters of the bottom scintillation plane (T_2 not present) or the two particles intersect scintillation counters in supermodules read out by different data acquisition systems (for a small fraction of the time, the electronics to synchronize the information between the supermodule readout systems was non-functional). Because the timing error seen in these events can be accounted for, all 37 are classified as muon plus up-going pion events and are included in the subsequent analysis.

The total path length between the two scintillation counter hits, given by the path length of the muon from the scintillator T_2 to $\vec{x}_v$ plus the path length of the pion from $\vec{x}_v$ to the scintillator T_3, is determined for events in the final data sample which satisfy

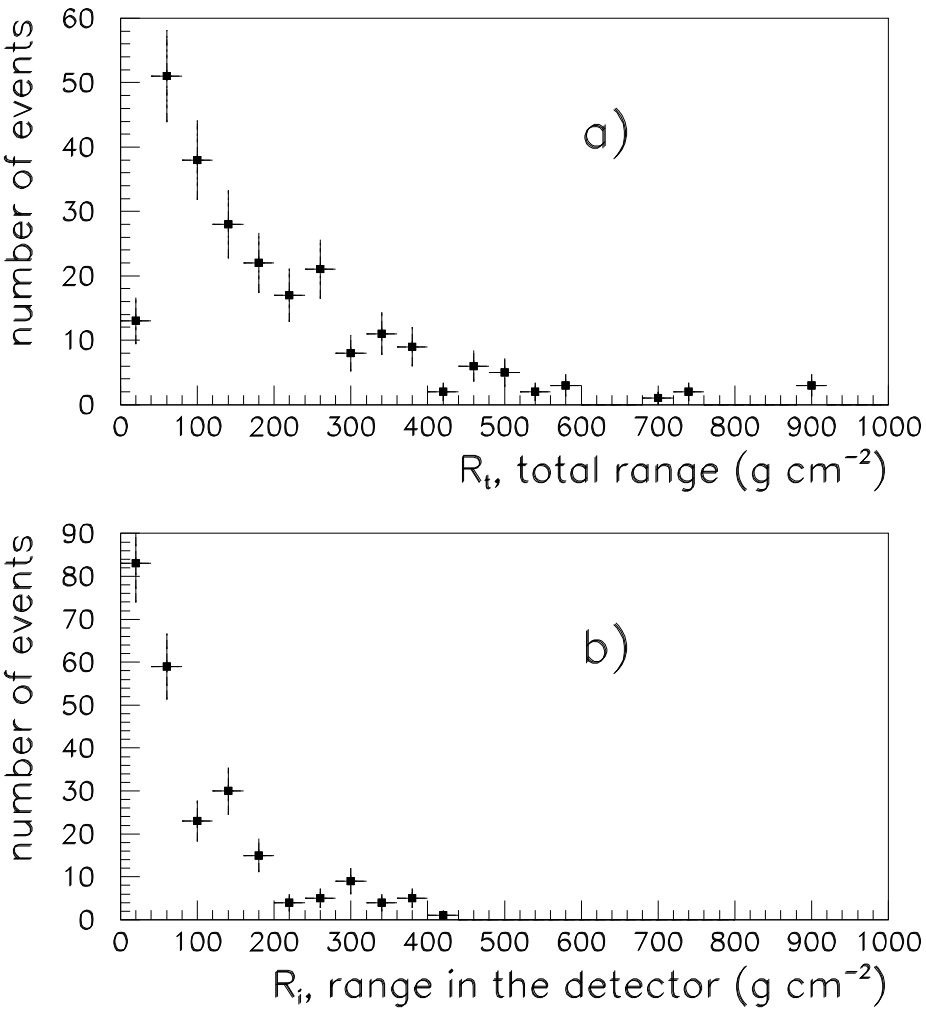

Figure 4: a) Distribution of the reconstructed total range R_t of the up-going particles for which $|z_v^w - z_v^s| < 50\ cm$. Events with a poorly reconstructed vertex are excluded from this distribution because of the large uncertainty in R_t for these events. b) Distribution of the grammage traversed in the detector, R_i, for all the 243 up-going particles in the final data set.

the condition $|z_v^w - z_v^s| < 50\ cm$. The correlation between the total path length and the time delay $(T_3 - T_2)$ is shown in Fig. 3. The linear correlation seen in this figure is consistent with the hypothesis that the up-going particle is produced at the vertex point. The uncertainty in the total path length depends on the uncertainty in the vertex location, and ranges from 50 cm up to 250 cm for the worst. The average uncertainty in the time delay between the two scintillation counters is approximately 2 ns for this data set.

The range of the up-going particle, R_t, is defined as the distance between the interaction point $(\vec{x}_v)$ and the position of the uppermost streamer tube hit in the track, $(\vec{x}_s)$. The range obtained in this way is, in most cases, an underestimate of the true range of the pion, by an amount as large as the vertical depth of the concrete absorber layer between streamer tube planes, 60 $g\ cm^{-2}$. The particle range is calculated by dividing the path length from $\vec{x}_v$ to $\vec{x}_s$ into 200 steps and considering the density of the material at each step. The sum of the product of the density times the step length gives the total range in $g\ cm^{-2}$. This procedure makes use of a detailed description of the distribution and density of the material inside and around the apparatus. In Fig. 4a the distribution of the total range of the pion, R_t, is shown. Only muon plus up-going pion events satisfying the condition $|z_v^w - z_v^s| < 50\ cm$ are included in this distribution. The

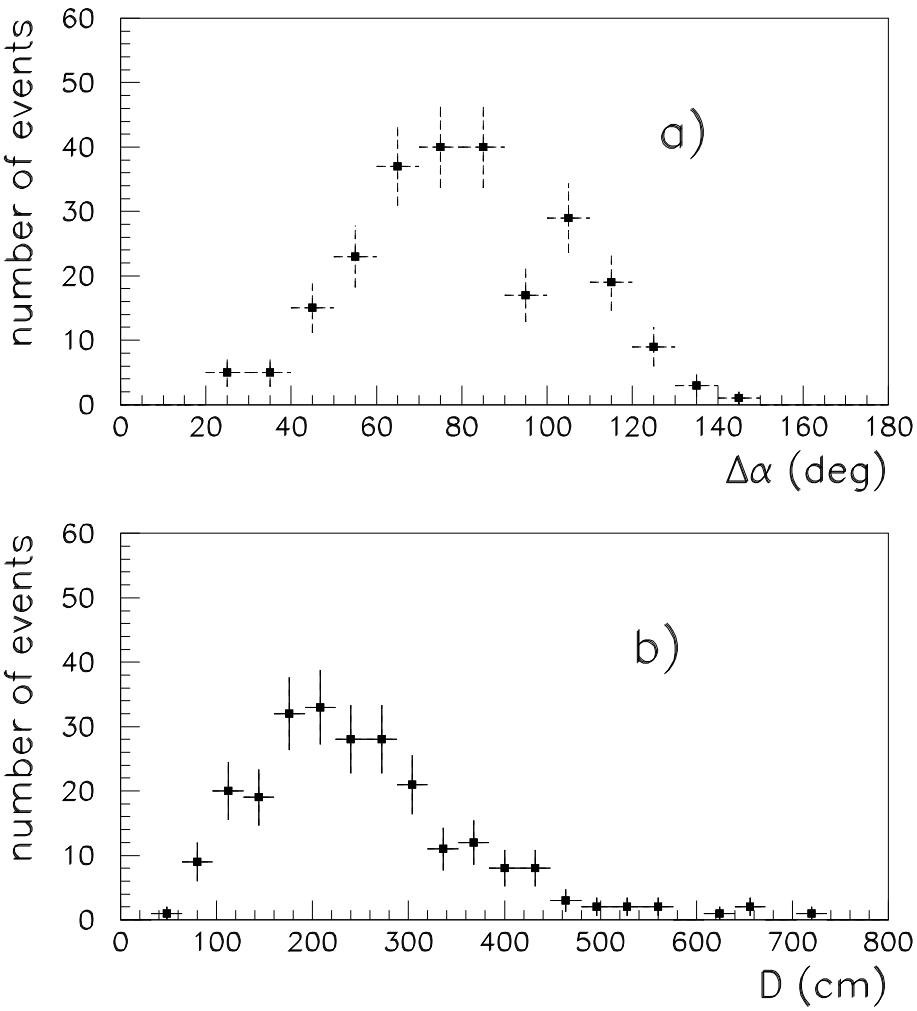

Figure 5: a) Measured distribution of the $\pi - \mu$ scattering angle $\Delta\alpha$ and b) of the distance D between the down-going muon and the up-going pion at the z location of the center of the bottom layer of scintillation counters.

partial range, R_i, of the up-going particle inside the apparatus is also calculated, and is shown in Fig. 4b. R_i is calculated from the bottom of the detector to the last active streamer tube hit in the up-going track. All the 243 muon plus up-going pion events are included in Fig. 4b, since the position of the vertex is not used in the calculation of R_i. It can be seen from these figures that a significant fraction of these events contain an up-going particle which penetrates enough material to be incorrectly identified as an up-going muon when the down-going particle is undetected.

Fig. 5a shows the measured distribution of the pion emission angle, $\Delta\alpha$, while Fig. 5b shows the distribution of the distance D between the muon and the up-going pion at a vertical position corresponding to the center of the bottom layer of the scintillator counters. The distributions, as discussed in the next section, decrease for small D as a result of a low event reconstruction efficiency, and for small $\Delta\alpha$ as a consequence of the low muon rate at large zenith angle. The radial distance between the muon and the up-going pion is less than 4 m, corresponding to roughly one third of the lateral size of one MACRO supermodule, in 90% of the events, as discussed in Section 7.

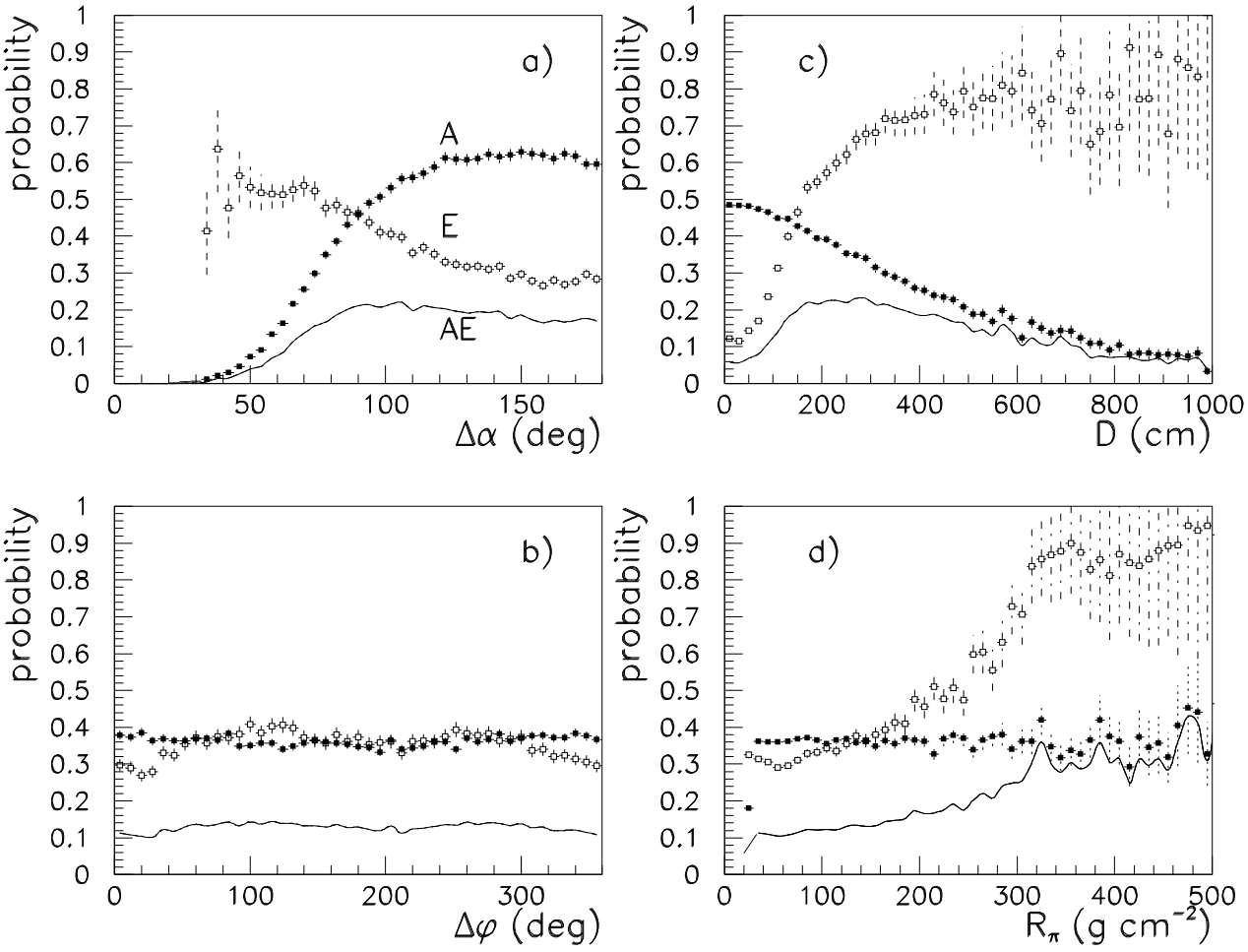

Figure 6: Distribution of the probability A for events to be accepted, of the tracking efficiency E, and of the reconstruction efficiency AE versus (a) $\Delta\alpha$, (b) $\Delta\varphi$, (c) D, and (d) R_π. Each quantity is averaged over the three remaining variables. Full points: A; empty points: E; solid curves: AE.

5. Reconstruction Efficiency

The probability of detecting an up-going pion produced by a down-going muon depends on the emission angles of the pion with respect to the muon, the pion energy, and the vertex depth. To determine the detection probability for these events in MACRO, a sample of 5.0×10^5 simulated muon plus up-going pion events is distributed uniformly over cells in the parameter space $\mathcal{P}$ defined by the variables $\Delta\alpha, \Delta\varphi, z_v$ and the pion range R_π (see Fig.2). The zenith angle $\Delta\alpha$ of the pion with respect to the incoming muon direction is constrained to lie in the range $0^o < \Delta\alpha < 180^o$. The vertex location $\vec{x}_v$ is taken at random locations below the detector, with the vertex depth at a distance $5 < d_v < 205$ cm from the bottom layer. The pion range inside the lower detector is chosen between $0 < R_\pi < 1000$ $g\ cm^{-2}$. This corresponds to a value of the pion momentum at the detector surface, p_π, in the interval $0.1 < p_\pi < 2.0$ GeV/c. In each simulated event, the down-going muon direction $(\vartheta_\mu, \varphi_\mu)$ is extracted from the measured distribution of atmospheric single muons. The point at which the muon enters the detector is distributed uniformly over the detector surface. The pion direction, $(\vartheta_\pi, \varphi_\pi)$, is given by $\vartheta_\pi = 180^0 - \vartheta_\mu - \Delta\alpha$ and $\varphi_\pi = \varphi_\mu - \Delta\varphi$. Using the events uniformly distributed on respect these parameters, and the actual angular distribution of the muons

at MACRO depth, the reconstruction efficiency, averaged on the muon directions, has been obtained as a function of the chosen parameter set.

GMACRO [6], a GEANT-based [7] Monte Carlo of the MACRO detector, is used to model the response to these particles. It describes the experimental apparatus (*i.e.* geometry, density, and the detector response) in all its details. The propagation of low-energy pions is potentially sensitive to the treatment of charge-exchange and in-flight absorption reactions. For this reason, the propagation of pions in the detector using the GEANT-GHEISHA (G-G) hadronic interface has been compared with results using the GEANT-FLUKA (G-F) interface (see [7] for references). We find that the two models give essentially the same detection probability for muon plus up-going pion events. For example, G-F predicts that a 500 MeV pion entering the detector from the bottom layer has a 20% probability of a range within the detector smaller than 25 $g\ cm^{-2}$, while G-G predicts a probability of 23%. This range corresponds to the minimum distance required to identify the up-going pion, and as a consequence, the number of accepted events does not differ significantly for the two cases. On the other hand, the energy distribution of the up-going pions, unfolded from the measurement of the range, is quite different for the two models. This can be illustrated by noting that the same 500 MeV pion has a probability of 57% of having a range smaller than 100 $g\ cm^{-2}$ in G-F, while G-G predicts a 74% probability. In the following, we report the results obtained with the GEANT-FLUKA simulation.

The result of processing the simulated muon plus up-going pion events in GMACRO is an output data set whose format is essentially identical to that of real data. This data set has been processed with the analysis chain used for the real data, described in section 4. A simulated event is defined as *accepted*, if the down-going muon is tracked and if the pion enters the detector and crosses the lower two horizontal streamer tube planes and the horizontal scintillator layer in between. The minimum amount of material traversed by a pion satisfying this requirement is $\sim 25\ g\ cm^{-2}$. The event is defined as *tracked* if the pion track is reconstructed, as described in Section 2. The acceptance probability and tracking efficiency for the simulated events is now obtained for each cell in the parameter space $\mathcal{P} = (R_\pi, \Delta\alpha, \Delta\varphi, D(z_v))$. The radial distance D is uniquely determined for a given pion and muon directions $(\vartheta_\pi, \varphi_\pi)$, $(\vartheta_\mu, \varphi_\mu)$ and vertex depth z_v. The acceptance probability for an event is defined as

$$A(R_\pi, \Delta\alpha, \Delta\varphi, D) = \frac{number\ of\ accepted\ event}{number\ of\ simulated\ events} \tag{2}$$

while the tracking efficiency is defined as

$$E(R_\pi, \Delta\alpha, \Delta\varphi, D) = \frac{number\ of\ tracked\ events}{number\ of\ accepted\ events} \tag{3}$$

Fig. 6 shows the acceptance probability A, the tracking efficiency E, and the reconstruction efficiency AE as a function of $\Delta\alpha$, $\Delta\varphi$, D and R_π. In each case, the values of A and E are obtained by averaging over the remaining three variables. Referring to Fig. 6, very few pions emitted with a small $\Delta\alpha$ (Fig. 6a) are detected, due to the fact that these pions must be produced by a near-horizontal muon, and the integrated muon flux with $\vartheta_\mu > 75^o$ is 6×10^{-3} of the total. In Fig. 6c, the decrease in the tracking efficiency for small D is a result of the merging of the pion and the muon tracks. Finally, the reconstruction efficiency increases as a function of the pion range within the

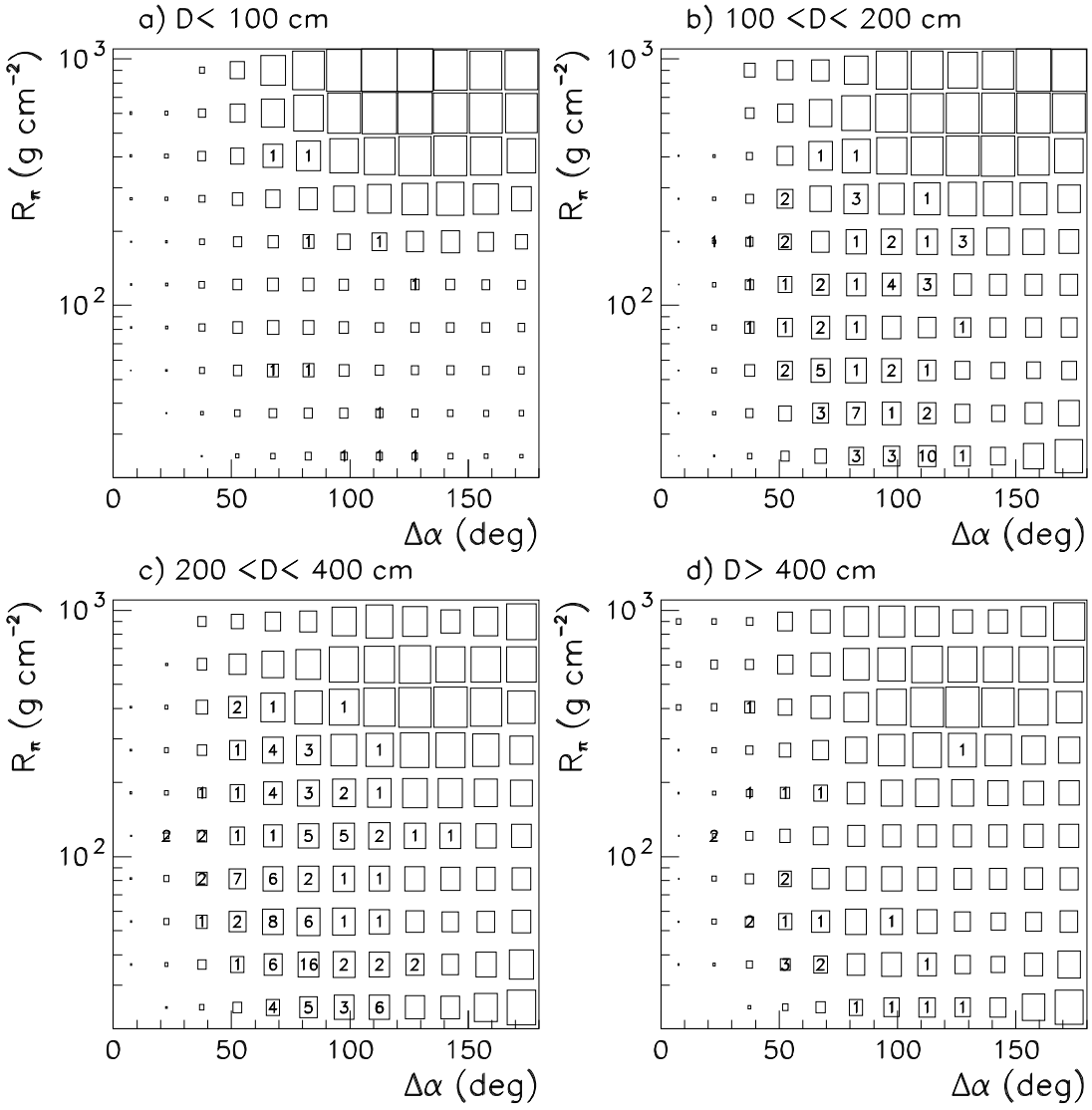

Figure 7: Reconstruction efficiency AE in the $(R_\pi, \Delta\alpha, D)$ parameter space, for 4 intervals of the distance D, 12 bins of $\Delta\alpha$ and 10 bins of the measured range of the pion inside the detector R_π. The computed values of AE are proportional to the box area. For example, the upper row in (d) corresponds to values of $(AE \cdot 100)$ equal to $1, 1, 3, 18, 29, 48, 52, 47, 40, 30, 48$ and 76. In each cell the number of detected muon plus up-going pion events at the given $(R_\pi, \Delta\alpha, D)$ values is indicated.

detector (Fig. 6d), because the tracking efficiency increases with the number of streamer tube hits in the track. Since (Fig. 6b) AE is essentially independent of the azimuthal scattering angle $\Delta\varphi$, it is assumed in the following that $AE = AE(R_\pi, \Delta\alpha, D)$.

In Fig. 7, the value of AE is shown as a function of R_π and $\Delta\alpha$ in four intervals of the distance D: (a) $D < 100\ cm$, (b) $100 < D < 200\ cm$, (c) $200 < D < 400\ cm$ and (d) $D > 400\ cm$. The box sizes are proportional to the reconstruction efficiency AE for detecting an event at a given (R_π,$\Delta\alpha$,D). In the same figure, the numbers inside the boxes correspond to the distribution of real events. In the four intervals of D there are 11, 78, 130 and 24 detected events with a muon plus an up-going pion, respectively. The number of detected events $N_{det}(i, j, k)$ in each cell of Fig. 7 can be considered as the convolution (plus statistical fluctuations) of the reconstruction efficiency $AE(i, j, k)$ with the unknown physical distribution of the events as a function of the variables in the parameter space $\mathcal{P}$. To obtain these physical distributions, we evaluated the corrected number of events as the number of detected events in each cell divided by the reconstruction efficiency: $N_{corr}(i, j, k) = N_{det}(i, j, k)/AE(i, j, k)$. Because of the uncertainties

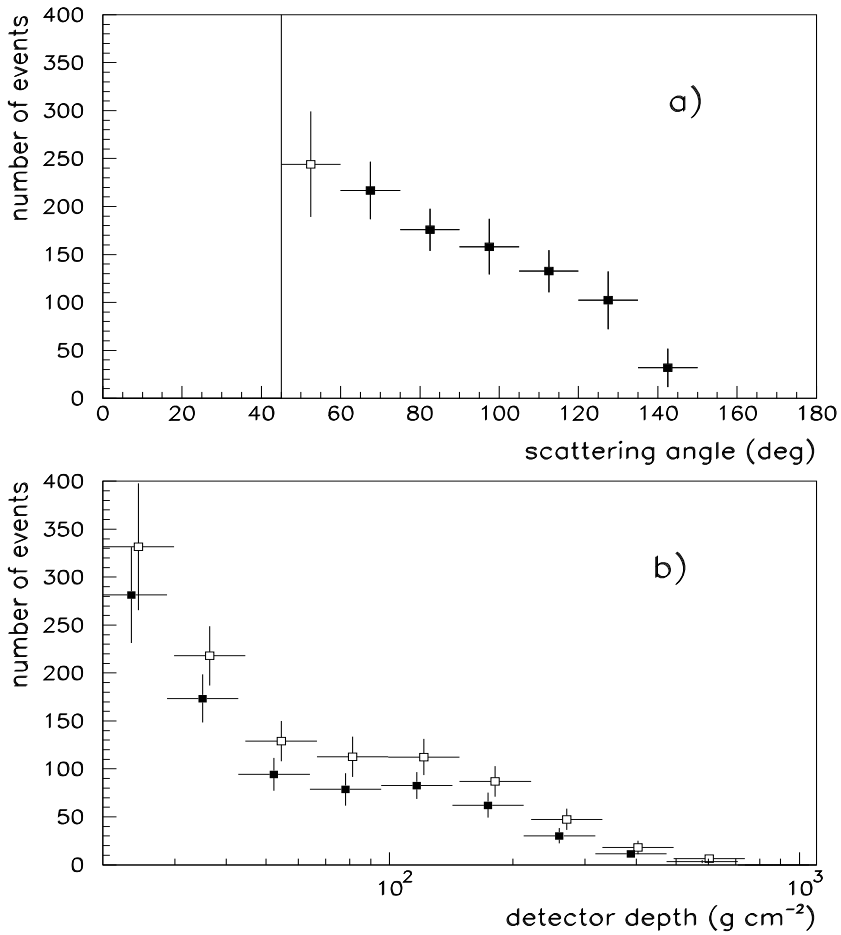

Figure 8: a) Detector-unfolded distribution of the zenith scattering angle $\Delta\alpha$ of the pion with respect to the muon direction, for $\Delta\alpha > 45^o$. b) Detector-unfolded distribution of the up-going pion range inside the detector. Open points: pions with $\Delta\alpha > 45^o$; full points: pions with $\Delta\alpha > 60^o$ (b). Only statistical errors are shown. The number of events corresponds to 1.55 y of data taking.

in the reconstruction of $\Delta\alpha$ and R_π from the measured track parameters, there is a small probability that an event in the (l, m, n) cell of $(R_\pi, \Delta\alpha, D)$ will be measured in the (i, j, k) cell. This probability, which results in a smearing of the $N_{det}(i, j, k)$ distribution, has been evaluated using the simulated sample. The mean detection efficiency for $\Delta\alpha > 45^o$, averaged over the other parameters of $\mathcal{P}$, is found to be

$$\epsilon_r = \sum_{i,j,k} N_{det}(i, j, k) / \sum_{i,j,k} N_{corr}(i, j, k) = (21 \pm 2_{stat} \pm 4_{sys})\% \qquad (4)$$

The systematic uncertainty is estimated by examining the effect of changing the sizes of the $(R_\pi, \Delta\alpha, D)$ cells, and by evaluating the difference in the results obtained using the two hadronic interfaces to GEANT.

From the distribution $N_{corr}(i, j, k)$, we obtain the detector-unfolded distribution of the pion-muon zenith scattering angle $\Delta\alpha$ and of the pion range inside the detector R_π. The two distributions, which correspond to the x and y projection of $\sum_k N_{corr}(i, j, k)$, respectively, are shown in Fig. 8. Given the low probability for events to be detected at small pion emission angles, the $\Delta\alpha$ distribution is shown for $\Delta\alpha > 45^o$.

Fig. 9 shows the angular distribution of up-going charged particles versus $cos(\vartheta)$, where ϑ is the zenith angle in the detector frame. The distribution is normalized to the total number of down-going single muons (12.2×10^6), and is corrected for reconstruction efficiency.

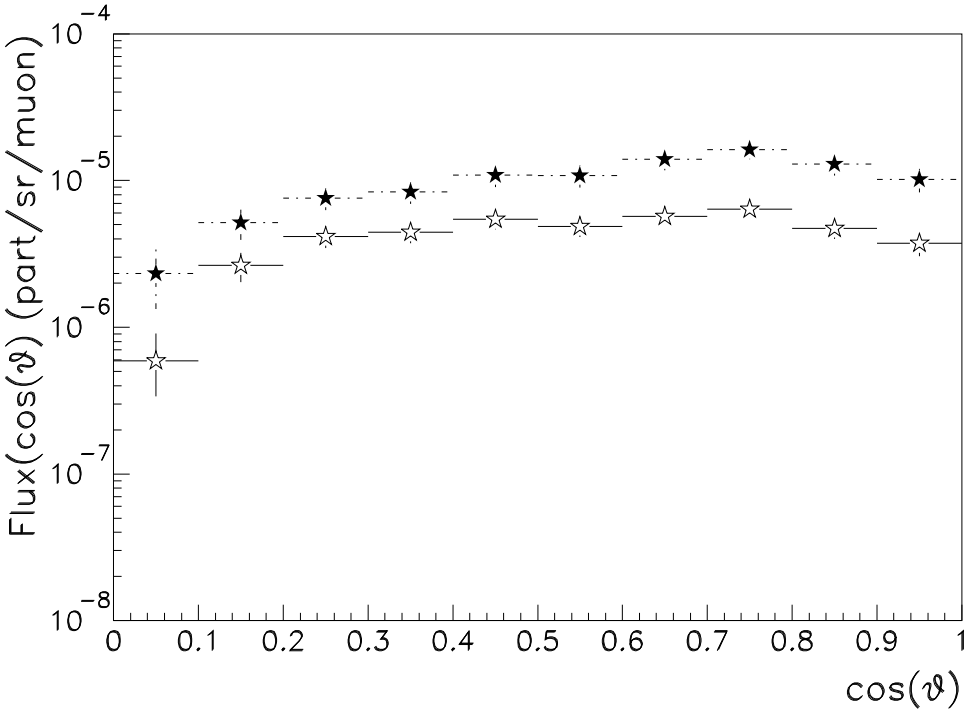

Figure 9: Angular distribution of the charged particles emerging from the floor, ϑ, relative to the vertical direction. The flux is normalized to the total number of detected single muons (12.2×10^6). Open stars: uncorrected data. Full stars: corrected and detector-unfolded data for pions with scattering angles $\Delta\alpha > 45^o$. The pion energy threshold is around 100 MeV. Only statistical errors are shown.

Using the detected number of muon plus up-going pion events and the mean detection efficiency quoted above, the estimated number of up-going pions emerging from the floor at the MACRO depth with angle of scattering $\Delta\alpha > 45^o$ with respect to the muon direction and range > 25 $g\ cm^{-2}$, per down-going muon is found to be

$$N_{\pi/\mu} = \frac{n_{\pi/\mu}}{\epsilon_r} = (10^{+4}_{-2.5})\ 10^{-5} \tag{5}$$

6. A Model of High Energy Muon Interactions

To compare with the results of the previous section, estimates of pion production by underground muons have been made using the hadronic interaction generator FLUKA[8] combined with a model of hard muon scattering with the muon photonuclear cross sections of Ref. [9]. The implications of this process for muon energy loss are discussed in [10]. The muon photonuclear cross section for the average muon energy at the MACRO depth is $\sigma_\gamma(\overline{E}_\mu \sim 280\ GeV) \simeq 0.40\ mb$. This corresponds to a probability of 0.3% for a 300 GeV muon to have one hard scattering in one meter of rock. σ_γ does not depend strongly on energy. For example, $\sigma_\gamma(E_\mu = 1000\ GeV) \simeq 0.55\ mb$.

In [9] the interaction cross section for a muon of a fixed energy is given in terms of the fractional energy loss and of the q^2 transferred. Hadron production by muons is computed in the framework of the Weizsäcker–Williams approximation [11] for the radiation of virtual photons, and the vector dominance model. Measured photon-vector meson couplings are used. Some uncertainties and limitations of the simulation arise

from the fact that deep inelastic scattering is not included in FLUKA. However, this process is dominated by low q^2 interactions. In addition, although bremsstrahlung, pair production and other electromagnetic interactions of muons are considered, the transport of secondary e^+e^- and γ is not performed. Therefore, electromagnetic showers are not produced, nor is photo-production by real photons considered.

The differential energy spectrum $G(E_\mu, h)$ of muons at the MACRO depth, along with the interaction model discussed above, have been used to estimate the flux of hadrons produced by muons at MACRO. An analytic approximation of $G(E_\mu, h)$ [12] is used, which assumes that the atmospheric inclusive muon spectrum above 1 TeV is described by the power law $\Phi(E_\mu) = KE_\mu^{-\gamma}$,and gives a differential muon spectrum underground at the effective average depth h of $G(E_\mu, h) = Ke^{-\beta h(\gamma-1)}\left(E_\mu + \epsilon\left(1 - e^{-\beta h}\right)\right)^{-\gamma}$, with γ=3.7, β=0.4 $(km\ w.e.)^{-1}$ and ϵ=540 GeV [12]. The average value of the rock overburden for MACRO, weighted by the measured muon flux, is $h = 3.8\ km.w.e.$. Due to the shape of the rock overburden, there is a correlation between residual energy and angle. This correlation is neglected in the model.

To simulate the production of up-going pions under MACRO, the muon energy is extracted from the energy spectrum shown above in the energy range $1\ GeV < E < 10\ TeV$. An interaction of the muon in the rock floor is then modeled, and the energy spectrum of the up-going particles exiting the floor is determined. All possible muon interactions are allowed, and the full hadronic cascade development is considered. For each particle type, the yield as a function of the kinetic energy and emission angle is then determined. We find that, as expected, the charged particle yield is dominated by charged pions, and that the differential pion spectrum decreases sharply with the kinetic energy and the emission angle $\Delta\alpha$. The charged kaon contribution is found to be lower than the pion contribution by about one order of magnitude. Protons (and neutrons) have an energy spectrum which is considerably softer than that of pions.

Next, in order to determine the number of muon plus up-going pion events due to this process observed in MACRO, muons with the energy distribution shown above are generated in (45×180) cells of $(\vartheta_\mu, \varphi_\mu)$ using the intensity/depth relation given in [13], and the slant depth obtained using a rock map of the Gran Sasso mountain (see [13]). The measured density of the Gran Sasso rock ($\rho = 2.657\ g/cm^3$) is used in place of the usual standard rock. The absolute muon flux observed by MACRO provides the overall normalization for the simulation. Each simulated atmospheric muon undergoes a hard scattering in the rock around the apparatus. Only pion production is considered, according to the differential pion yield $Y_{\pi/\mu}(E_\pi, \Delta\alpha)$ obtained by the simulation procedure above. The generated pions are then propagated to the apparatus. A simulated sample equivalent to 1.2×10^8 detected single muons was generated, corresponding to $N_y = 14.4\ y$ of full detector livetime.

Taking into account the real probability for hard scattering by an atmospheric muon, the predicted rate of muon plus up-going pion events in which both particles enter in the detector is $(8 \pm 3)\ 10^{-5}\ \pi/\mu$. The quoted error includes the uncertainty in the muon flux, the pion yield and the pion propagation in the detector. This result is in agreement with the measured value, quoted in Section 5.

7. Evaluation of the Background due to Up-going Pions in Neutrino Studies.

The flux of atmospheric muon neutrinos $\Phi_{\nu(\mu)}$ is often inferred from a measurement of the flux of up-going muons. MACRO can measure $\Phi_{\nu(\mu)}$ in the 100 GeV region using through-going muons and, in the $5-10$ GeV region, using stopping muons. An up-going pion induced by an interaction of a down-going atmospheric muon in the rock around the detector results in a background event in the neutrino measurement if the muon is undetected.

The rate of events in which the down-going muon is not detected, and in which the up-going pion simulates a neutrino-induced muon, has been evaluated using the simulation described in the previous section. In the simulated sample, equivalent to 14.4 y of data taking, 63 events are seen in which the up-going pion crosses two scintillator layers and the muon is undetected. Of these, 31 events contain pions which traverse more than 200 $g\ cm^{-2}$ of detector material. These events satisfy all of the criteria [14] for an upward through-going muon. This gives a background rate due to up-going pions of

$$Upward\ throughgoing\ \mu\ background\ =\ (2.1 \pm 0.4_{stat} \pm 0.7_{sys})\quad events/year$$

The expected number of detected up-going muons from ν_μ interactions in the rock below MACRO is approximately 200 $events/year$[14], giving a contamination from this background of approximately 1%. The distribution of the cosine of the zenith angle of these background events is essentially flat.

Partially contained muon neutrino interactions in the apparatus, giving rise to a down-going muon, and up-going stopping muons induced by a ν_μ interaction in the rock below the apparatus, are identified by applying appropriate constraints to the observed tracks [15]. In the following, these events are called *stopping muons*. The background for the stopping muon sample is evaluated by applying the analysis of ref. [15] to the simulated events. 127 events are found in which the up-going pion satisfies the criteria used in this analysis for the identification of stopping muons, and in which the muon is not observed. This corresponds to a rate of these background events of

$$Upgoing\ stopping\ \mu\ background\ =\ (8.8 \pm 0.9_{stat} \pm 0.8_{sys})\ events/year$$

The expected rate of stopping muons is about 80 $events/year$ in MACRO, implying a contamination by up-going pions in this sample of about 10%.

The background rates obtained above are specific to the MACRO detector. For smaller detectors, the probability of detecting the pion while missing the muon increases. For example, for a single MACRO supermodule the background/signal ratio for the through-going sample is almost twice the value quoted above. Other underground experiments measuring neutrino-induced muons should have a similar contamination due to up-going pions, with the exact background rate depending on the geometrical configuration of the detector, its depth, and on the momentum threshold applied to the up-going muons. To our knowledge, no experiment measuring the flux of atmospheric neutrinos using up-going muons (see references in [14]) has taken into account this background. In particular, shallower experiments for similar energy threshold should have a significant contamination from these events, because the average muon energy, $\overline{E}_\mu(h)$, and the corresponding pion yield, $Y_{\pi/\mu}$, decreases slowly with decreasing depth, while the total muon flux increases exponentially.

8. Conclusion

In this paper we report the first measurement of up-going particles associated with down-going atmospheric muons in an underground detector. This measurement was possible because of the large area, good tracking and good time measurement capabilities of the MACRO apparatus.

In 12.2×10^6 downgoing single muons we find a total of 243 events with an identifiable up-going particle spatially and temporally associated with a down-going muon. We have analyzed the experimental distributions of *i*) the total range of the pion from the production point to the stopping point, *ii*) the pion range inside the detector, *iii*) the $\pi - \mu$ zenith scattering angle and *iv*) the radial distance between the two particles in the bottom layer of scintillators.

The probability A of events to be accepted, the tracking reconstruction efficiency E and the reconstruction efficiency AE in cells of the parameter space $\mathcal{P}(R_\pi, \Delta\alpha, \Delta\varphi, D)$ have been evaluated using a Monte Carlo simulation of the detector. This allows the calculation of the mean detection efficiency ϵ_r for events in which the $\pi - \mu$ scattering angle $\Delta\alpha > 45^o$. We find $\epsilon_r = (21 \pm 2_{stat} \pm 4_{sys})\%$. We have presented the detector-unfolded distributions of the $\pi - \mu$ zenith scattering angle $\Delta\alpha$, of the detector material thickness crossed by the upgoing particles, and of the angular distribution of charged particles emerging from the floor in the detector frame. The measured rate of up-going pions with range $R_\pi > 25$ $g\ cm^{-2}$ per down-going muon at the Gran Sasso depth, corrected for the reconstruction efficiency of the MACRO apparatus, is $N_{\pi/\mu} = (10^{+4}_{-2.5})\ 10^{-5}$.

A comparison of the data with a Monte Carlo calculation of up-going pion production in hard muon interactions shows good agreement in the measured pion production rate at the MACRO depth.

The up-going particles generated by interactions of down-going muons constitute a background source for neutrino induced events. For MACRO, the background rate is $(2.1 \pm 0.4_{stat} \pm 0.7_{sys})$ $events/year$ for the upward through-going sample with a muon energy threshold of ~ 400 MeV, corresponding to 200 $g\ cm^{-2}$ of detector. It is $(8.8 \pm 0.9_{stat} \pm 0.8_{sys})$ $events/year$ for the up-going stopping sample. This background is of the order of 1% of the through-going muons and of the order of 10% of the up-going stopping muons.

Acknowledgements

We gratefully acknowledge the staff of the *Laboratori Nazionali del Gran Sasso* and the invaluable assistance of the technical staffs of all the participating Institutions. For generous financial contributions we thank the U.S. Department of Energy, the National Science Foundation, and the Italian *Istituto Nazionale di Fisica Nucleare*, both for direct support and for FAI grants awarded to non-Italian MACRO collaborators.

References

[1] J.W. Elbert, M.Iacovacci and V.Silvestrini, Europhys. Lett. 14 (1991) 181.

[2] M. Treichel, Z. Phys. C **54** (1992) 469.

[3] O.G. Ryazhskaya, JEPT letters **60** (1994) 617.

[4] IMB Collaboration, R. Becker-Szendy et al., Phys. Rev. **D46** (1992) 3720; Kamiokande Collaboration, K.S. Hirata et al., Phys. Lett. **B280** (1992) 146.

[5] M. Cribier et al., Astrop. Phys. 6 (1997) 129.

[6] The MACRO collaboration, S.Ahlen et al., Nucl. Inst. and Meth. **A324** (1993) 337.

[7] R. Brun et al.,(GEANT3), CERN report DD/EE/84-1 (1987).

[8] A. Fassó et al., (FLUKA: present status and future developments), *Proc. of the IV Int. Conf. on Calorimetry in High Energy Physics,* La Biodola (Is. d'Elba), Italy, ed. World Scientific (1993) 493.

[9] L.B. Bezrukov and E.V. Bugaev, Sov. J. Nucl. Phys. 33 (1981) 635.

[10] W. Lohmann et al. (Energy loss of muons in the energy range 1-10000 GeV), CERN Yellow Report 85-03 (1985).

[11] C.F. Weizsäcker, Z. Phys. 88 (1934) 612.

E.J. Williams, Mat. Fys. Medd. Dan. Vid. Selsk. 4 (1935).

R.H. Dalitz and D.R.Yennie, Phys. Rev. **105** (1957) 1598.

[12] T.K. Gaisser, Cosmic Rays and Particle Physics, Cambridge University Press, Cambridge, England (1990).

[13] The MACRO collaboration, M. Ambrosio et al., Phys.Rev. **52D** (1995) 3793.

[14] The MACRO collaboration, M. Ambrosio et al., (Neutrino results using upward-going muons in MACRO), MACRO/PUB 96/4 (1996).

[15] S.P. Mikheyev (Detection of High Energy Neutrinos with MACRO), Proc. of the VIth Neutrino Telescope Workshop, Venice, p.493 (1994).